Progress In Electromagnetics Research C, Vol. 94, 29–44, 2019

Multi-Negative Index Band Metamaterial-Inspired Microfluidic Sensors

Nantakan Wongkasem* **and Mark Ruiz**

Abstract—Simple, compact and high sensitivity metamaterial-inspired microfluid sensors are developed to detect and classify dielectric fluids in the X-band regime using reflection coefficients. Multi-negative refractive index band metamaterial structure is specifically designed as a sensing enhancer, where the multi-negative bands can effectively trigger the electromagnetic properties, as well as enhance the differentiation between the testing samples. The geometry of the metamaterial enhancer and its arrangement with the microfluidic channel and radiating patch antenna are optimized to reach the highest sensitivity of the samples' depiction. The proposed sensors were tested on ethanol traces, where sets of complex permittivity were varied. Distinguishable frequency responses generated from different samples at four resonances specify the capability of classifying the fluid concentration.

1. INTRODUCTION

In recent years, an alternative sensing system, based on engineered materials or metamaterials (MTMs), MTM-inspired sensors [1–35], passive devices ranging from GHz to THz range, has been introduced for testing different substances such as solid (dielectric and metallic) materials [5, 14], liquids [2–4, 7, 9–13, 15–23], microparticles [8], and biomolecules [24, 35], to name a few. Microfluidic sensors [36] with their label-free, non-destructive characteristics, no-contact, instant measurements, low-cost, and low-profile [1, 2], can be a substitute for optical, electrochemical and biological sensors. It was also shown that a single negative MTM surface can have multifunctional usages, i.e., sensors and absorbers [22].

The fundamental principle of these MTM-inspired microfluid microwave sensors is correlated with the dielectric perturbation phenomenon. The electromagnetic boundary conditions are stimulated and resonated when a testing sample is integrated in the sensor system, resulting in: (i) the shift of the resonant frequency, associated with material polarization, and (ii) the change in quality (Q-) factors, related to the dielectric loss of material [2]. Both changes have been implemented to measure the relative complex dielectric constant or permittivity of the testing sample. In addition, based on various applications, ones may focus on four sensing strategies, i.e., (i) resonance frequency variation, (ii) coupling modulation through symmetry disruption, (iii) frequency splitting, also exploiting symmetry properties, and (iv) amplitude modulation of a harmonic signal [5].

MTM-inspired microfluid microwave sensors generally consist of a microstrip transmission line loaded with MTM structures and a fluidic channel of various shapes. Most MTM-inspired microfluidic sensor prototypes [1, 6, 18, 20] presented a similar testing setup preforming the transmission response measurements, where the complex permittivity extracted from the transmission (S_{21}) and reflection (S_{11}) coefficients is used to classify the testing material. The MTMs designed for specific electromagnetic properties are integrated into the sensor system in order to effectively manipulate the shift of the resonant frequency and the change in Q-factors, resulting in a more pronounced dielectric perturbation

Received 15 April 2019, Accepted 26 June 2019, Scheduled 11 July 2019
* Corresponding author: Nantakan Wongkasem (nantakan.wongkasem@utrgv.edu).
The authors are with the Department of Electrical and Computer Engineering, The University of Texas Rio Grande Valley, Edinburg, TX 78539, USA.

phenomenon. The MTMs, offering improved compactness and a high Q-factor, play a significant role in creating a bridge between the testing sample and the electromagnetic (EM) resonance. The fluidic channel between the inlet and outlet is designed to ensure a constant volume and shape of the fluid sample across the sensing area. The sensing capability and efficiency are directly influenced by the correlation between the MTM structures and the fluidic channel. To differentiate the sensing performance, symmetry properties in transmission line loaded with one or more MTM structures need to be considered to avoid the lack of coupling due to the complete cancellation between electric and magnetic fields [6, 37–40]. All the MTM structures implemented for microfluidic microwave sensors are either a split ring resonator (SRR), a complementary SRR (CSRR), an open SRR (OSRR), or a split-ring-cross resonator (SRCR) [1, 2–4, 7, 8, 10–13, 15–20, 22], which are typical magnetic resonators first introduced as negative permeability MTMs [41]. The inductive-capacitive (LC) resonance frequency of the SRR is determined by the inductance (L) of the ring and capacitance (C) of the gap region. Since C is a function of permittivity, any changes in the dielectric property of the material positioned in the gap region will change its effective C, thereby resulting in a spectral shift of the LC resonance [8]. These SRRs with various orientation, e.g., single-ring, double-ring, square, circular, or rectangular shape, can be easily designed to generate a magnetic resonance, where the negative real part of the permeability is located. A single magnetic resonance from the SRRs is normally narrow, resulting in a narrow sensing frequency band; for example, a 0.05 GHz band for a sensor with a 1GHz operating frequency [6]. 4-circular double SRRs with different dimensions have been designed for multi-bands in order to optimize the permittivity characterization [1]. Hence, different MTM structure types, for instance, negative refraction index (NRI) MTMs [42–44, 52], chiral MTMs [4, 45–47], and near-zero-index (NZI) MTMs [48, 49], can be additional choices, where more parameters can be manipulated.

In this article, we propose to design a multi-NRI band MTM to aid the sensing ability of the microfluid sensor in the X-band frequency range. The broad multi-NRI bands of the MTMs, generated from both electric and magnetic couplings, will furthermore assist the sensor to generate stronger multi-band transmission responses covering a broader frequency of interest, while testing a sample, hence more accurate and more detailed data will be obtained. While optimizing the MTMs orientation, the fluidic channel will be modified accordingly in order to cover all sensing areas, as well as to ensure a constant volume and shape of the fluid sample. Although a simple quarter wavelength transmission line is commonly used in most microfluidic sensors as a microwave transmission part, there was an attempt to implement a complementary SRR-loaded patch as an excitation port [12], where only reflection coefficients (S_{11}) were collected. In fact, a stand-alone patch antenna can be employed as a main sensing element [50]. In this research we also propose to implement a microstrip patch antenna as the only port to collect the reflection coefficient data. Since the patch antenna can be specifically designed to operate in a particular observing frequency range, more precise data can be obtained, which is adequate for detecting different sample types. However, if both transmission and reflection coefficients are required for some particular samples to further extract other electromagnetic properties, e.g., permittivity, permeability, chirality, refractive index, etc., another identical patch antenna can be set as a receiving port.

2. MICROSTRIP PATCH ANTENNA AND MICROFLUIDIC CHANNEL

While a simple quarter wavelength transmission line is commonly used in most microfluidic sensors as a microwave transmission part, in this research we propose to implement a microstrip patch antenna as the only port to collect the reflection coefficient or S_{11} data. Not only can the radiation pattern and beamwidth of the patch antenna be designed to focus on the microfluidic channel and the MTM enhancer, but also the observing frequency range can be controlled effectively. Therefore, more accurate data can be obtained, which is adequate for detecting different sample types.

2.1. X-Band Microstrip Patch Antenna

An X-band patch antenna was made by a two-sided 1 oz Cu FR-4 substrate with $\varepsilon_r = 4.4$, shown in Figure 4(a), where $a = 4.83$ mm, $b = 9$ mm, $c = 6.5$ mm, $d = 3.5$ mm, and $e = 3$ mm was designed for the X-band transmission. The transmission coefficients and the far-field of the patch are presented in

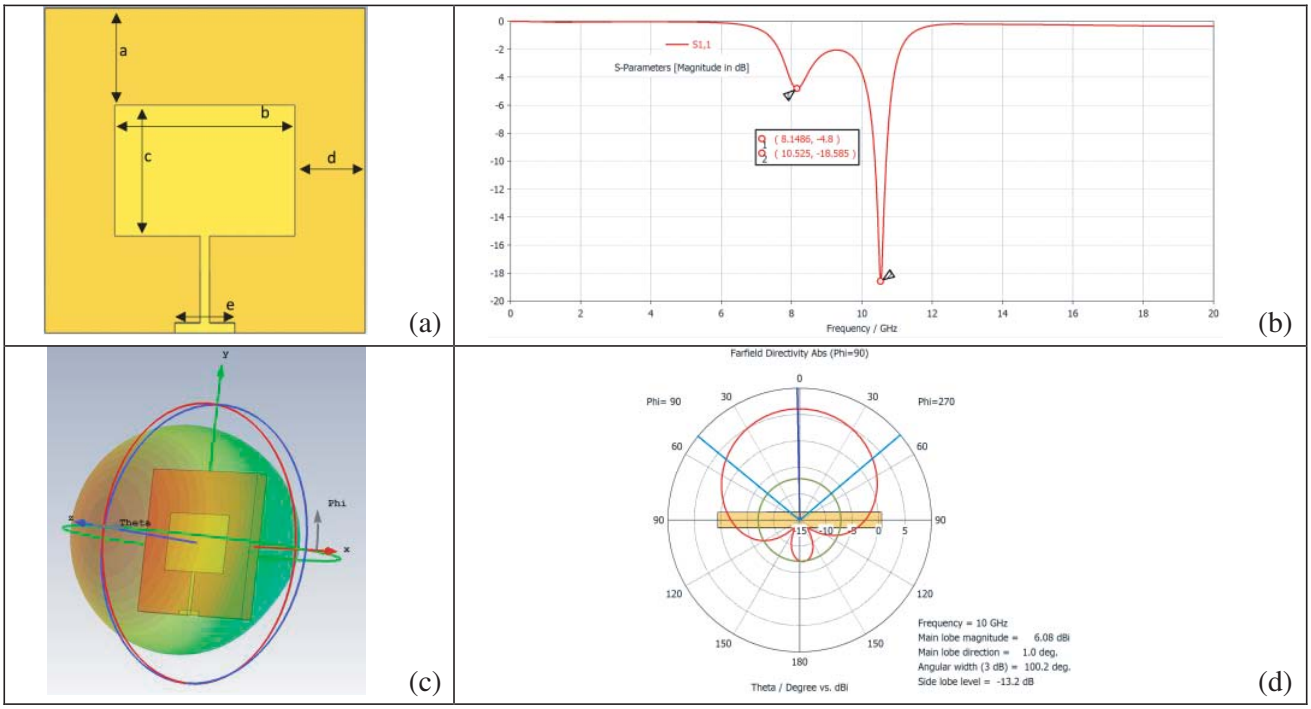

Figure 1. X-band patch antenna and its transmission coefficient and far-field distribution.

Figure 1.

There were two resonances of the reflection coefficient at 8.14 GHz (−4.8 dB) and 10.53 GHz (−18.59 dB), generated from this 9 cm × 6.5 cm patch antenna. The 3-dimensional (Figure 1(c)) and 2-dimensional (Figure 1(d)) far-field patterns indicate a good main lobe magnitude and direction within 8–12 GHz with the angular width of 100.2°.

2.2. X-Band Microstrip Patch Antenna and Sampling Fluid Layer

The patch antenna was then used to investigate its sensing responses, where a large $\lambda/15$ thin layer of ethanol of different concentrations [51] was placed on top of the radiating patch, as shown in Figure 2(a). The resonances of the sensing system depend on the permittivity of its surrounding materials. Therefore, when the testing fluid with different permittivities is included, the electric field is perturbed, and the resonant frequencies are changed. Figure 2(b) presents the far-field distribution recorded at 10 GHz

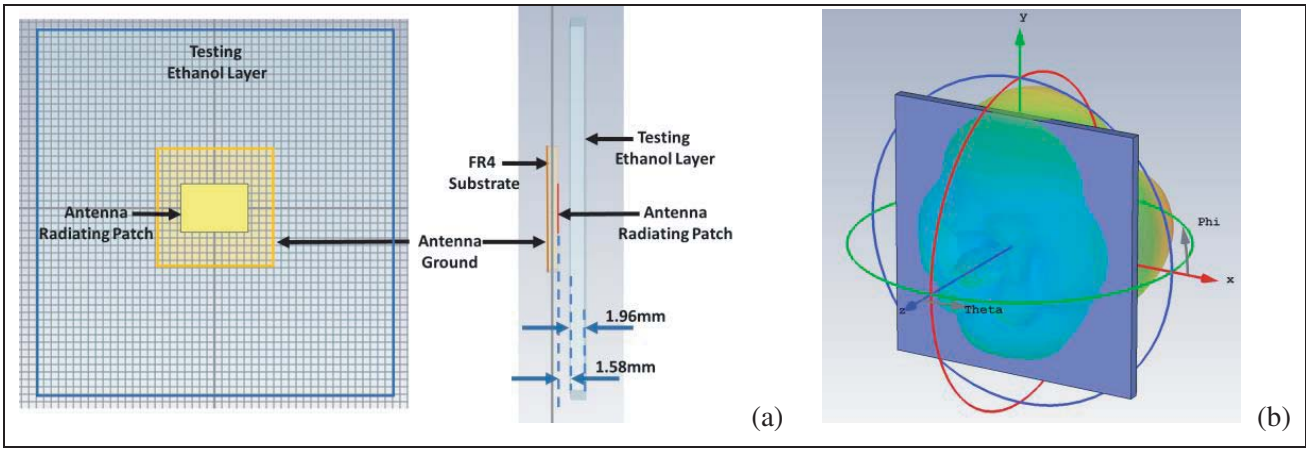

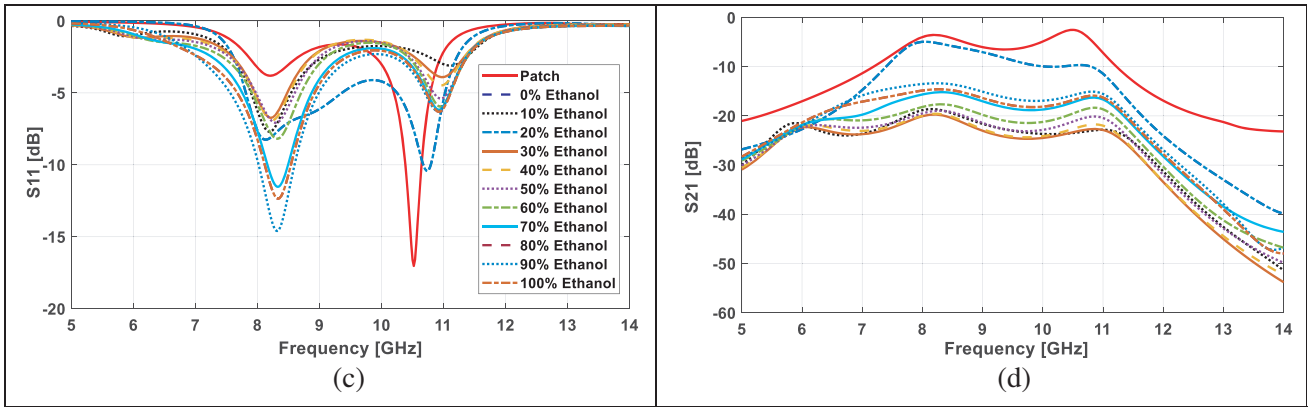

Figure 2. (a) Orientation of the patch and the testing ethanol layer. (b) Far-field distribution at 10 GHz from the 50% ethanol, and (c) the reflection and (d) transmission coefficients of the testing set.

from the 50% ethanol. The transmission (S_{21}) and reflection (S_{11}) coefficients collected from the patch and the testing ethanol layer are presented in Figures 2(c)–(d).

As the ethanol samples were tested, the two resonances were observed around 8 GHz and 10 GHz. Different transmission levels from different ethanol concentrations were found in the first dip, while the more obvious frequency shift in the second resonance was demonstrated.

These results are similar to those of multi-band double rings microfluidic sensors [1], where a pair

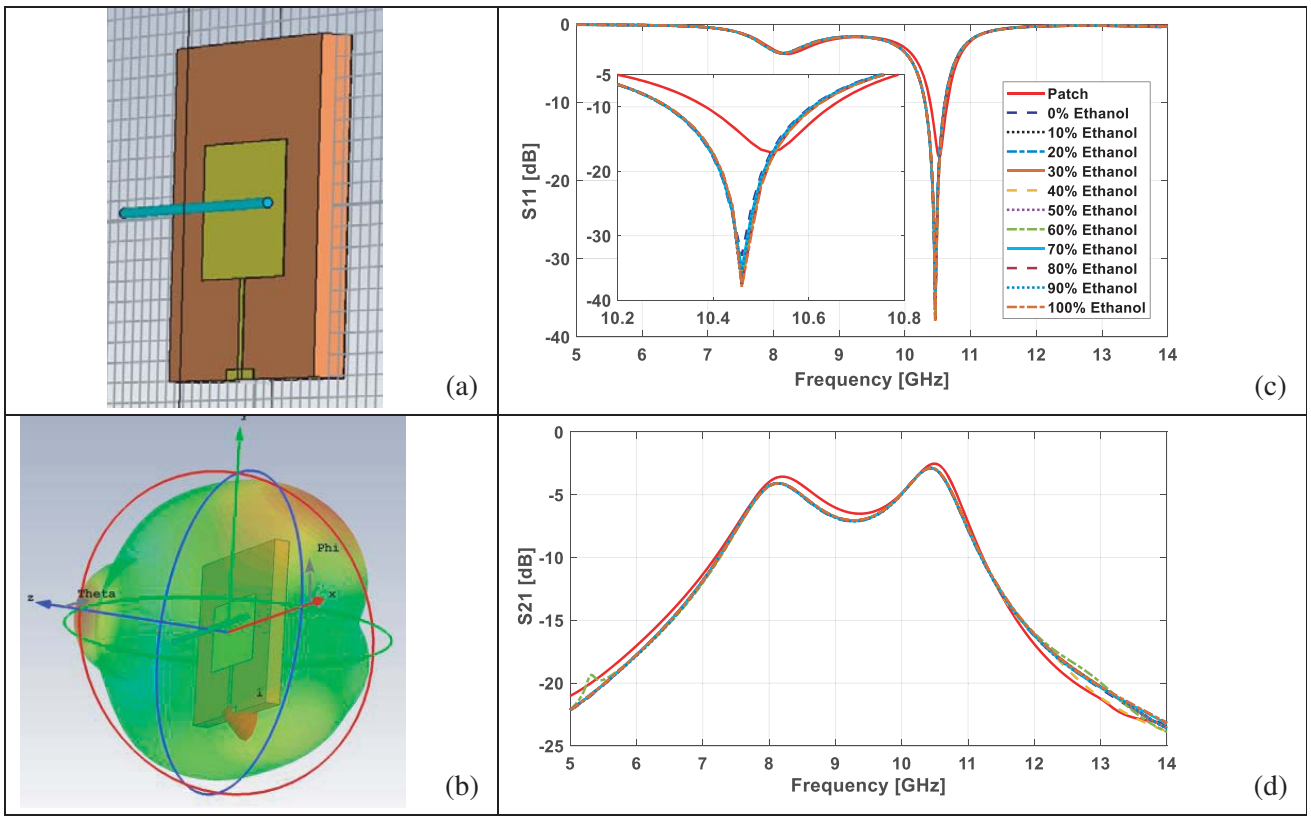

Figure 3. (a), (b) A 1-line fluidic channel and patch system and (c), (d) their sensing responses on different ethanol concentrations.

of resonances was also found, but at slightly lower frequencies. The differences mainly come from the different microwave transmission parts.

2.3. X-Band Microstrip Patch Antenna and Sampling Microfluidic Channels

To fulfill label-free and non-destructive purposes, instead of testing with the thin layer, three settings of a fluidic channel designed from a very simple one-line channel to four-line channel were implemented. The sensing capability of the antenna and microfluidic channels was investigated. The channel was created with a 0.5 mm diameter cylinder tube where the testing ethanol was later flowing through. The three sensing systems, and their transmission and reflection responses are presented in Figures 3–5.

Dual resonances were found in all three systems, though the more noticeable results, where different

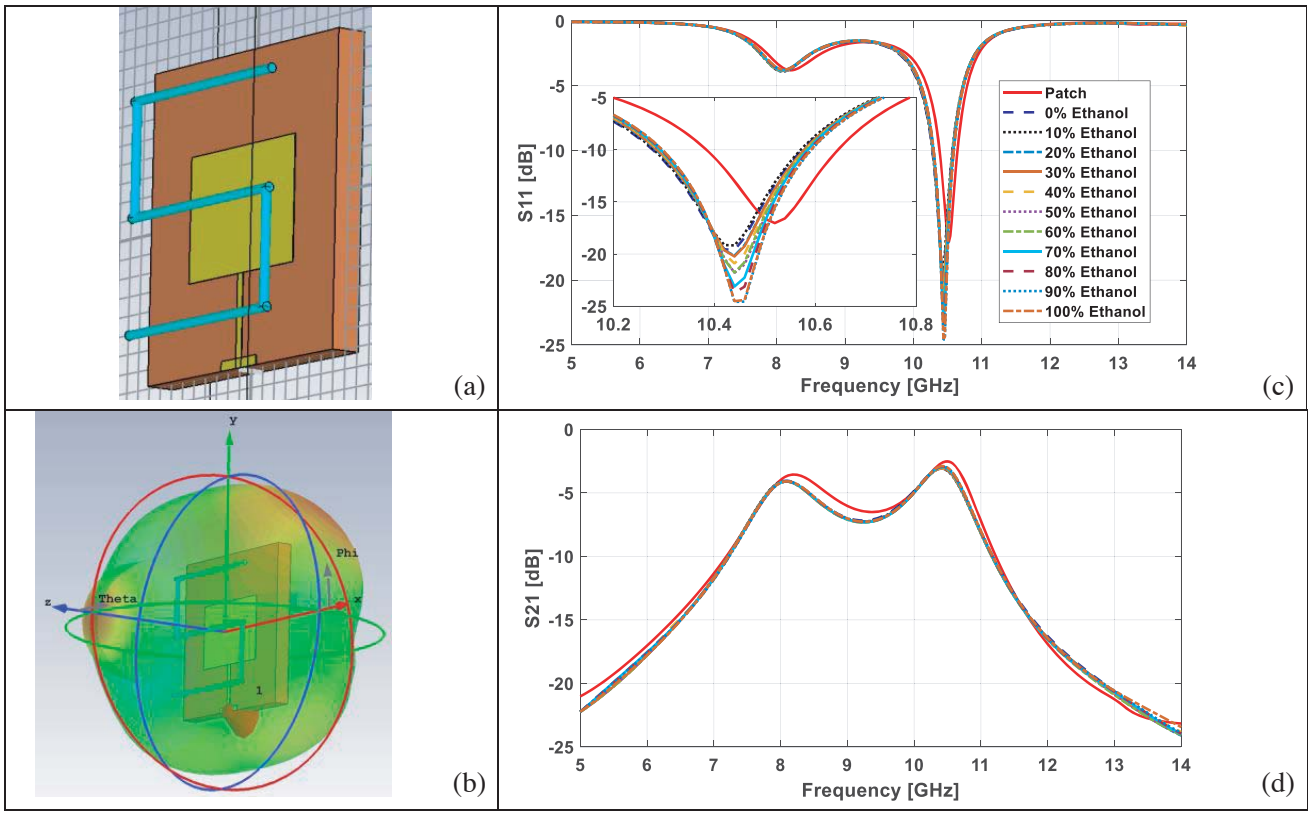

Figure 4. (a), (b) A 3-line fluidic channel and patch system and (c), (d) their sensing responses on different ethanol concentrations.

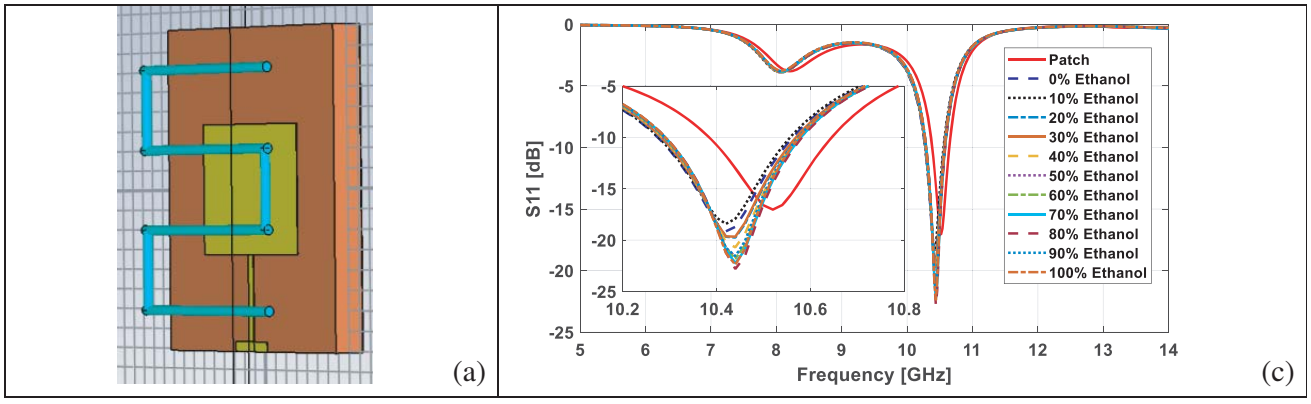

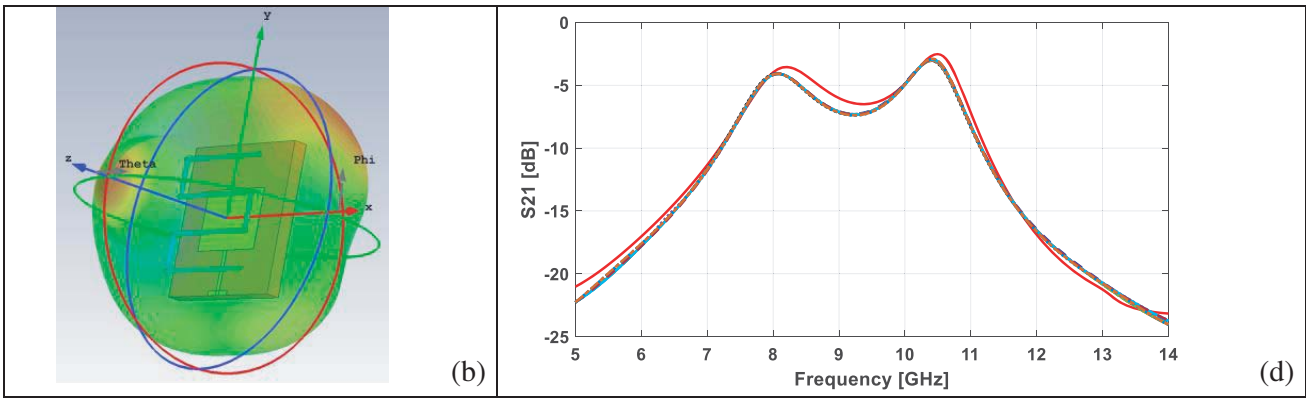

Figure 5. (a), (b) A 4-line fluidic channel and patch system and (c), (d) their sensing responses on different ethanol concentrations.

samples can be easily differentiated, were observed in both 3-line and 4-line channel sensor systems, as presented in the zoomed S_{11} results in Figures 3(c), 4(c), and 5(c).

This sensing aptitude is comparable to several literatures, where only single [12, 13, 17, 18, 20] and double resonances [1] were established while sensing ethanol traces in the microwave range. The level of this detecting performance may already satisfy several fluids with unpretentious properties; however, in order to improve the sensitivity and accuracy, extra bands (resonances) created from the proposed multi-negative-refractive-index (NRI) metamaterial structure will better serve the objective.

3. MULTI-NEGATIVE-REFRACTIVE-INDEX BAND METAMATERIAL

A multi-NRI band MTM structure, shown in Figure 6(a), is designed through various iterations of a complementary I-beam design, as the combination of an $(-)\varepsilon$ (epsilon or permittivity) and a $(-)\mu$ (mu or permeability) structure. The NRI band is generated from the overlap between a broad $(-)\varepsilon$ band and a magnetic resonance, where the resonance frequency (ω_m) is controlled by the total inductances (L_T) and total capacitances (C_T) of the MTM structure: $\omega_m = 1/\sqrt{L_T C_T}$. The conventional $(-)\varepsilon$

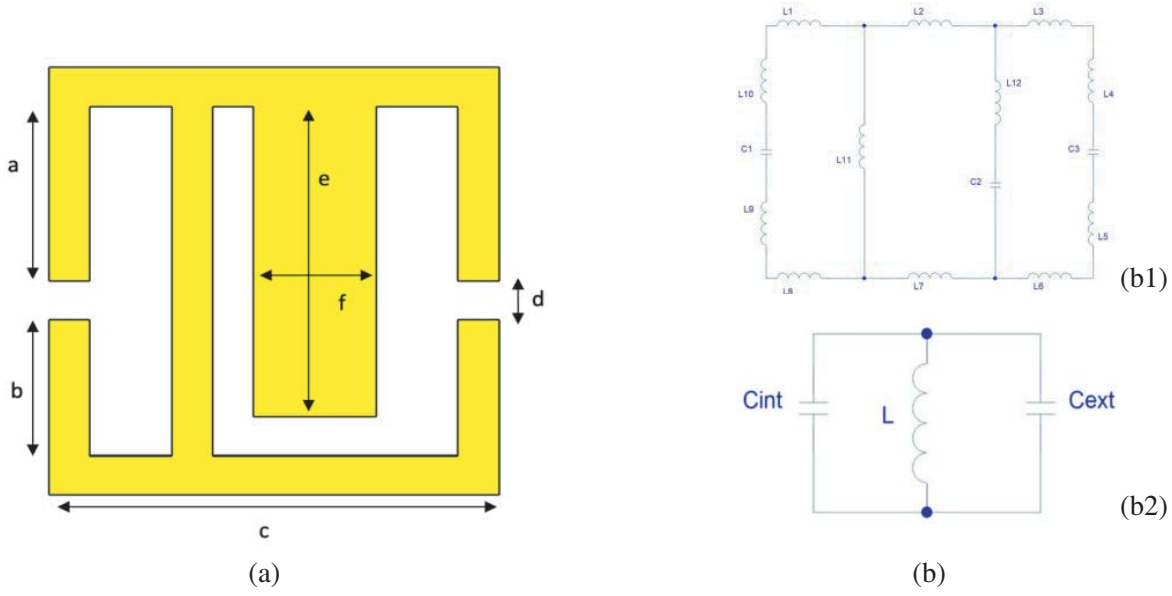

Figure 6. (a) Proposed multi-NRI band MTM structure and (b) its equivalent circuit.

structure is simply an array of straight conductive wires, where the wires must be set parallel to the electric field direction [52, 53]. On the other hand, the standard $(-)\mu$ structure is a magnetic resonator, where strong magnetic couplings, resulting in $(-)\mu$ response, is built between the magnetic field and its broken symmetric ring structure [39]. It was proved that the electric couplings can also create the

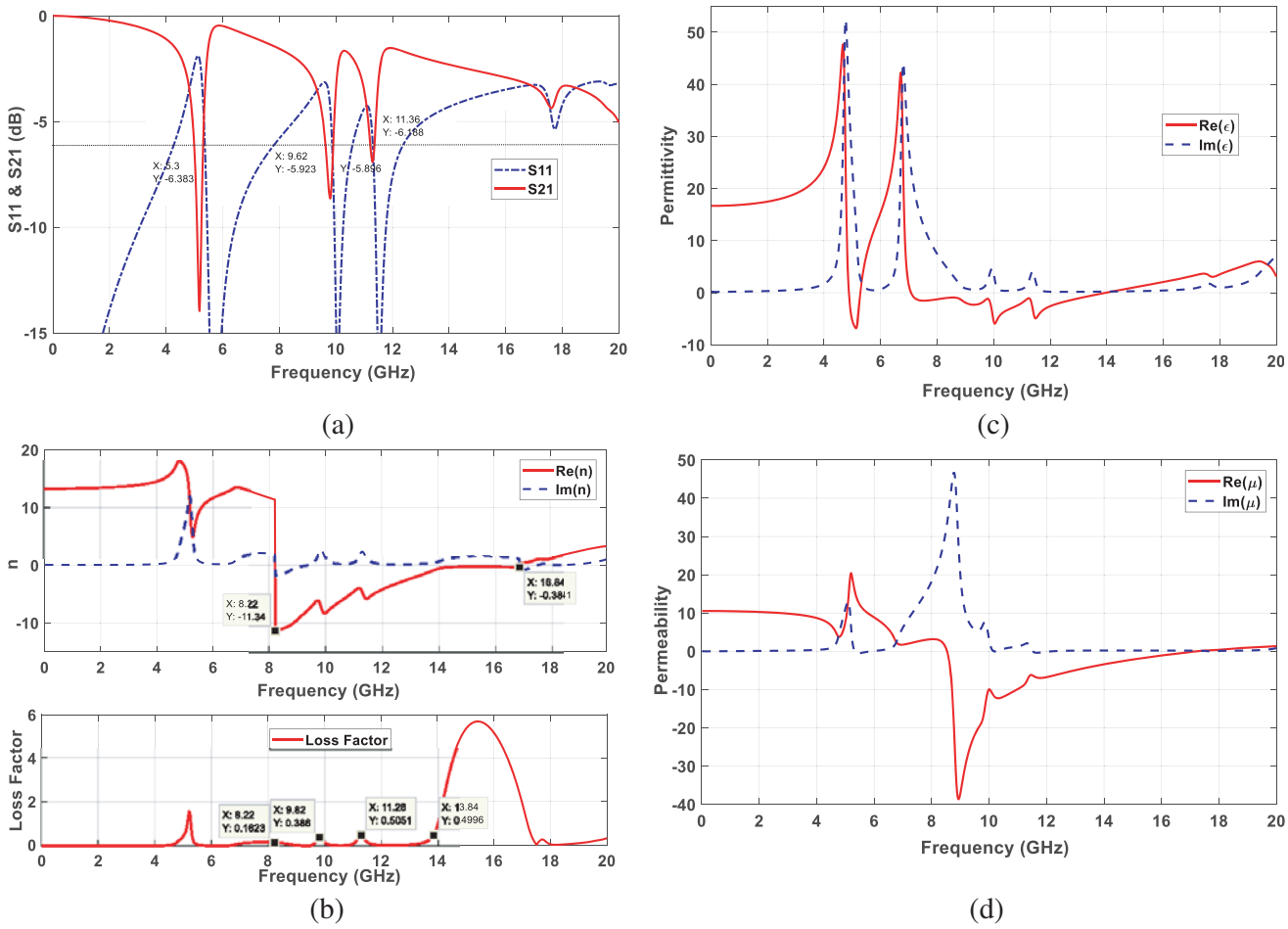

Figure 7. EM parameters of the multi-NRI band MTM: (a) S parameter, (b) refractive index and loss factor, (c) permittivity and (d) permeability.

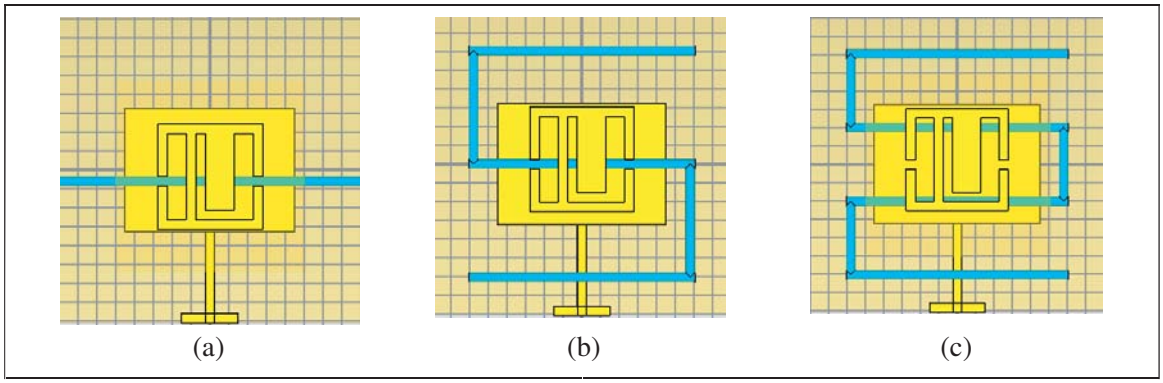

Figure 8. Patch antenna and NRI MTM with (a) 1-line, (b) 3-line and (c) 4-line microfluidic channel, and their far-field distribution when testing with the 50% ethanol at 10 GHz.

$(-)\mu$ [54], but a more careful EM field setting needs to be taken into consideration, i.e., the electric field must be parallel to the broken part or a gap of the structure. The advantage of this orientation choice is that the EM field direction can be set to be parallel to the structure plane. In order to create multiple NRI bands, a couple broken rings (split ring) of different sizes are required to generate multiple magnetic resonances.

An equivalent simplified circuit of the multi-NRI band MTM is presented in Figure 6(b1). Each inductance (L) represents the line segments of the MTM structure, whilst the generating gaps are

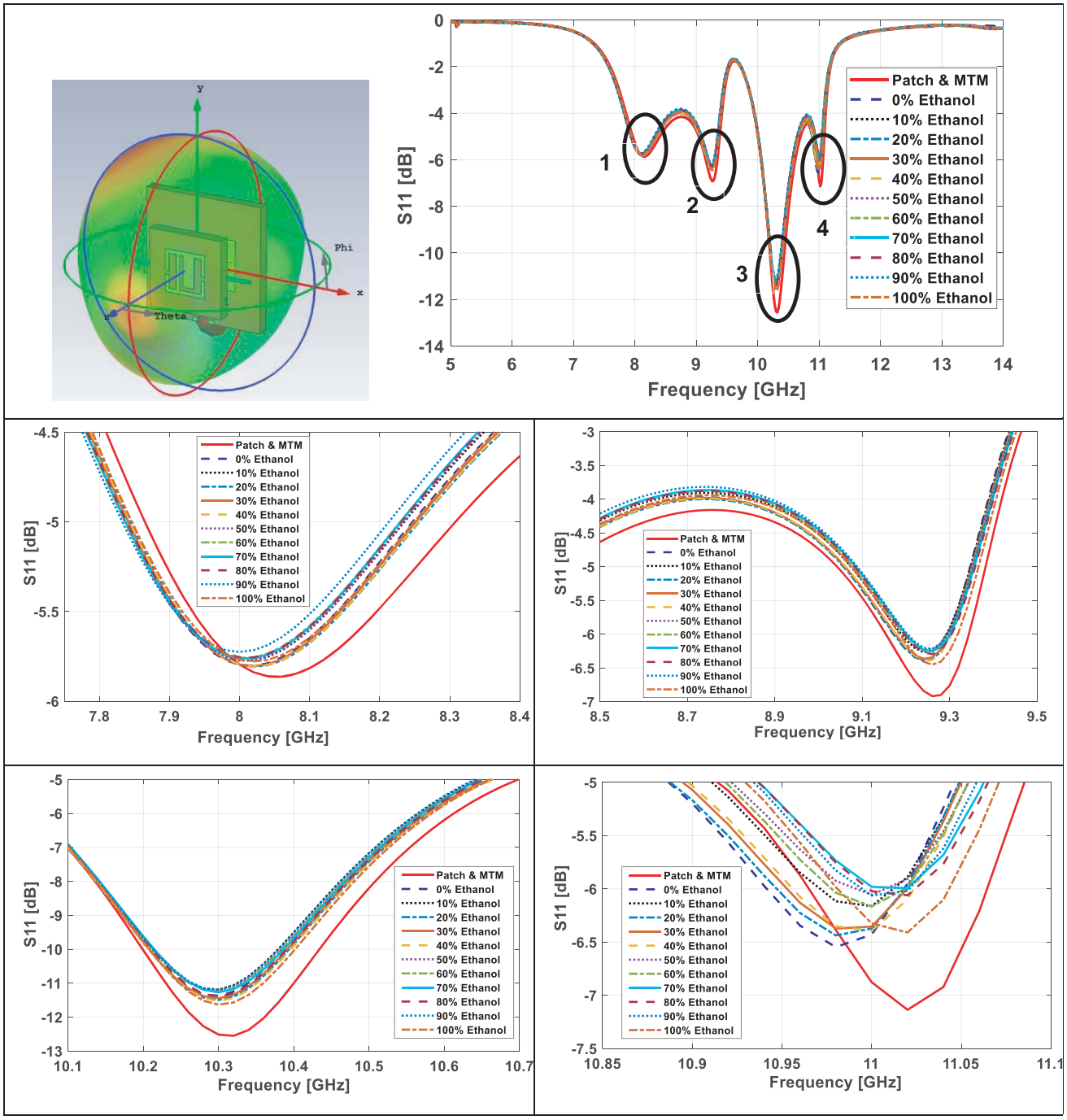

Figure 9. An MTM 1-line fluidic channel sensor system and their sensing responses on different ethanol concentrations.

represented by capacitances (C). These inductances and capacitances are added in series and in parallel depending on their respective nodes. The inductance and capacitance are calculated using an approximation for the self-inductance of a thin, conducting strip [55], and for a coplanar capacitor [56], respectively. When increasing the segment lengths, the total inductance increases, which has an inverse relation to the resonance frequency. Similarly, by decreasing the distance between segments, the capacitance increases, which also results in a shift of the resonance frequency to the lower end of the X-band. Depending on their series and parallel orientation, these components can be combined

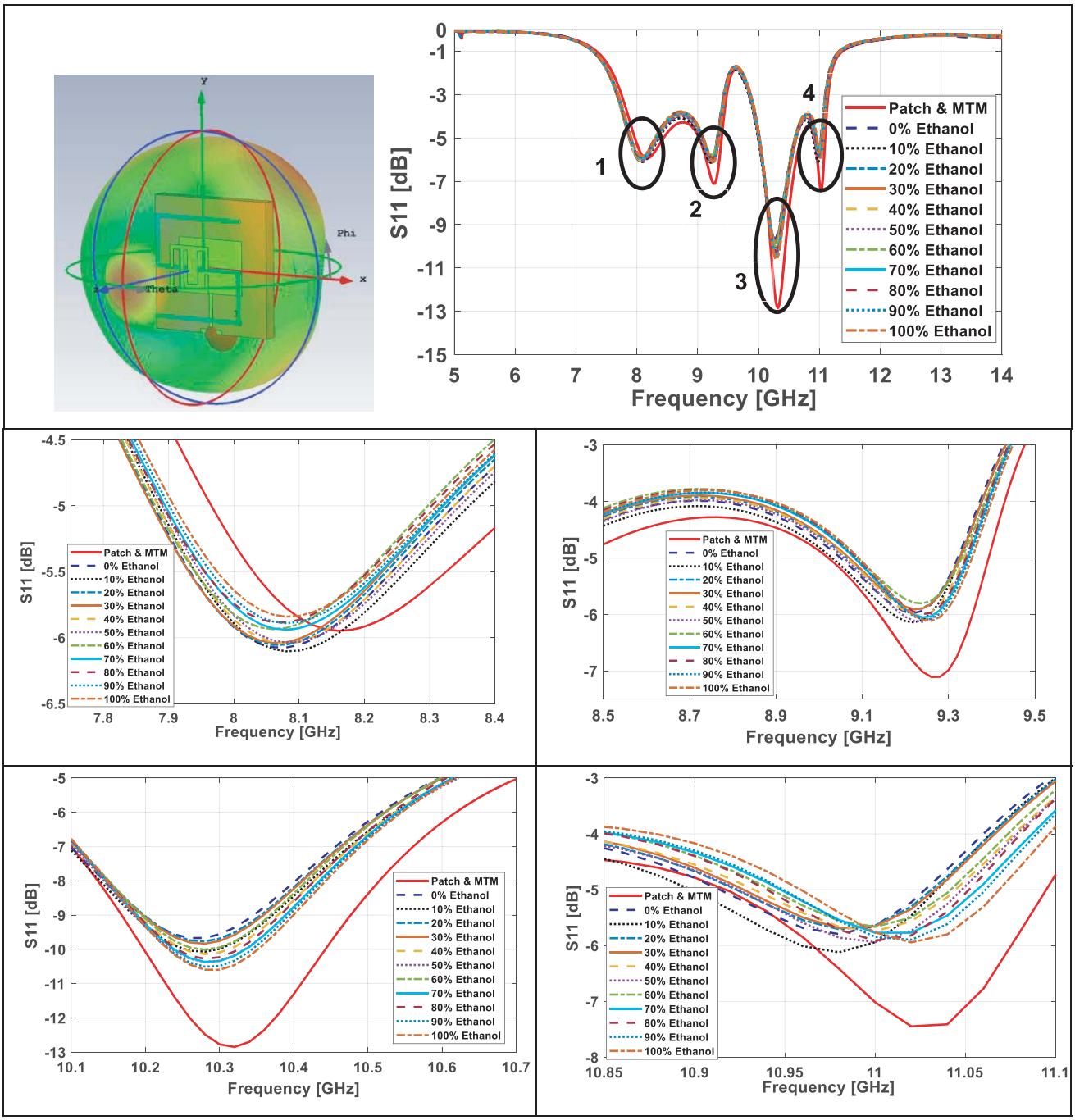

Figure 10. An MTM 3-line fluidic channel sensor system and their sensing responses on different ethanol concentrations.

to form a simplified circuit, as shown in Figure 6(b2), where C_{int} and L are the total C and L of an individual MTM structure, and C_{ext} is the capacitance created from adjacent structures [57].

The MTM structure is fabricated using a 10×10 mm FR-4 substrate ($\varepsilon_r = 4.4$) with a 1.54 mm thickness and loss-free copper with a 0.03 mm thickness. In order to control the operating frequency within the X-band frequency range, the MTM dimensions are designed as follows: $a = 2.25$ mm, $b = 1.75$ mm, $c = 6$ mm, $d = 0.5$ mm, $e = 1.5$ mm, and $f = 4$ mm, presented in Figure 6(a).

The S_{21} and S_{11} coefficients of the multi-NRI band MTM are presented in Figure 7(a). A good

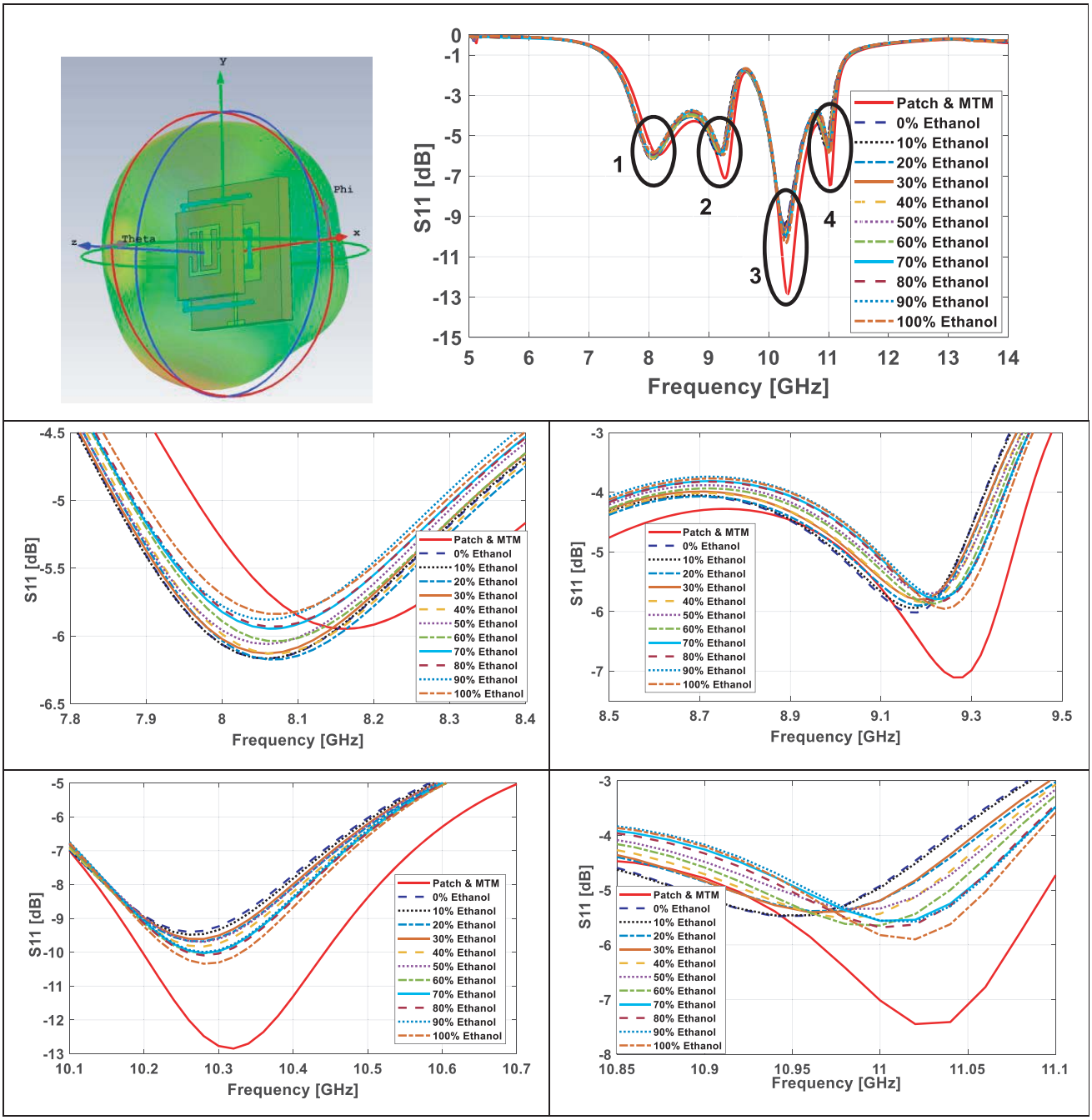

Figure 11. An MTM 4-line fluidic channel sensor system and their sensing responses on different ethanol concentrations.

transmission band of at least 50% transmission at −6 dB, observed from S_{21}, is generated covering all the X-band range, from 8 GHz to 14 GHz, with two narrow stopbands at 9.62 GHz and 11.36 GHz. These good transmission passbands are proved to have a negative index, the real part, from 8.22 GHz to 16.84 GHz, marked in the refractive index plot in Figure 7(b). The imaginary part of the refractive index, signifying material loss, is low within the operating range. Hence, the significantly low loss factor (LF), $LF = \frac{\text{Img}(n)}{\text{Real}(n)}$, less than 0.5, within the entire X-band, confirms the satisfactory transmission. The complex permittivity and permeability of the MTM are shown in Figures 7(c) and 7(d). The

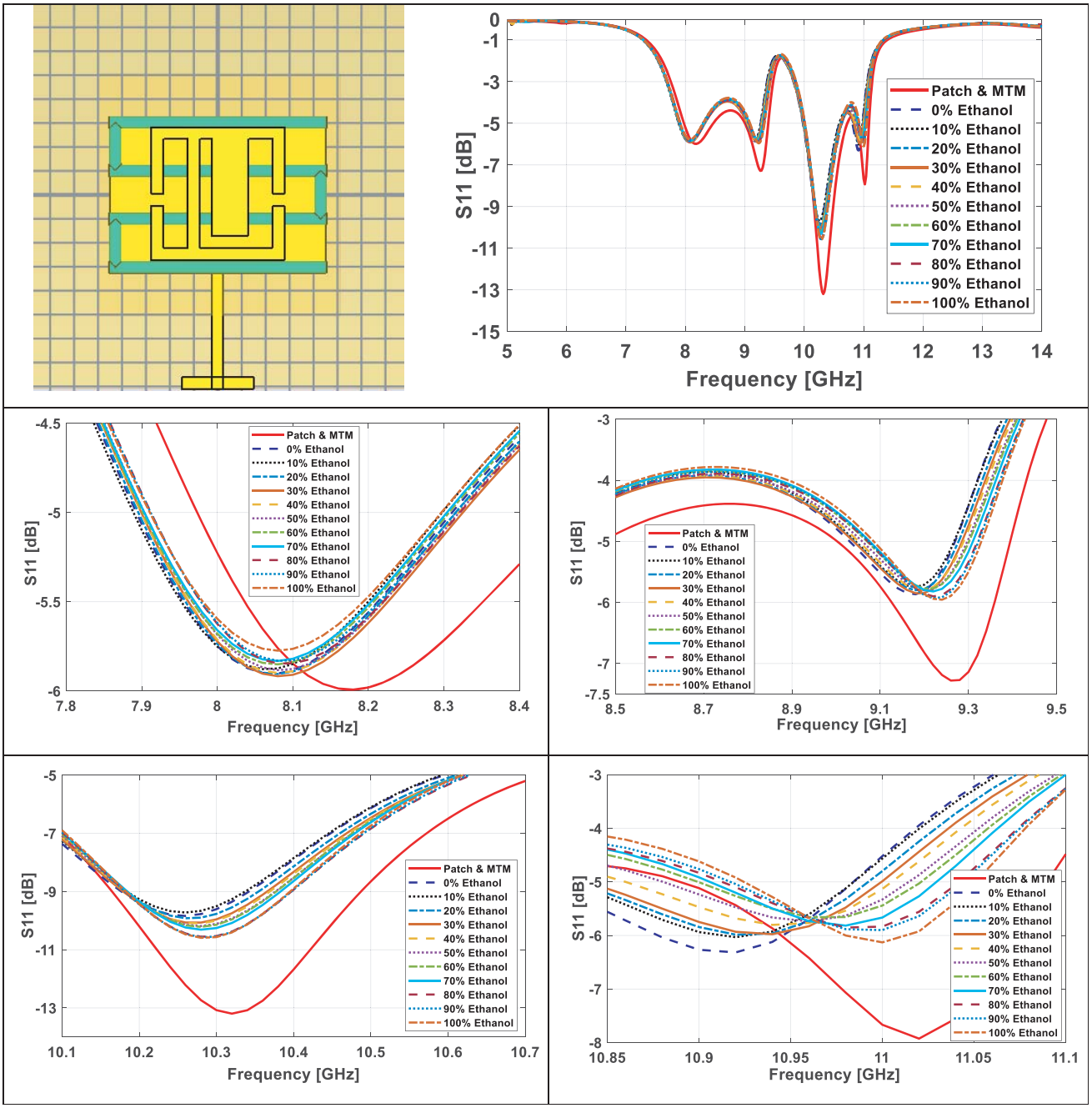

Figure 12. An optimized MTM 4-line fluidic channel sensor system and their sensing responses on different ethanol concentrations.

real part of both the permittivity and permeability are negative within the observing frequency range, confirming the NRI band. To effectively manipulate the NRI band, complex values of permittivity and permeability must be taken into consideration [58–60].

Within the operating frequency range, both electric and magnetic coupling responses are generated by the MTM structure, enhancing the interaction between the testing fluid and the EM wave, excited by the X-band patch antenna. In order to further improve the EM responses, the orientation, location, and dimensions of the microfluidic channel will need to be determined.

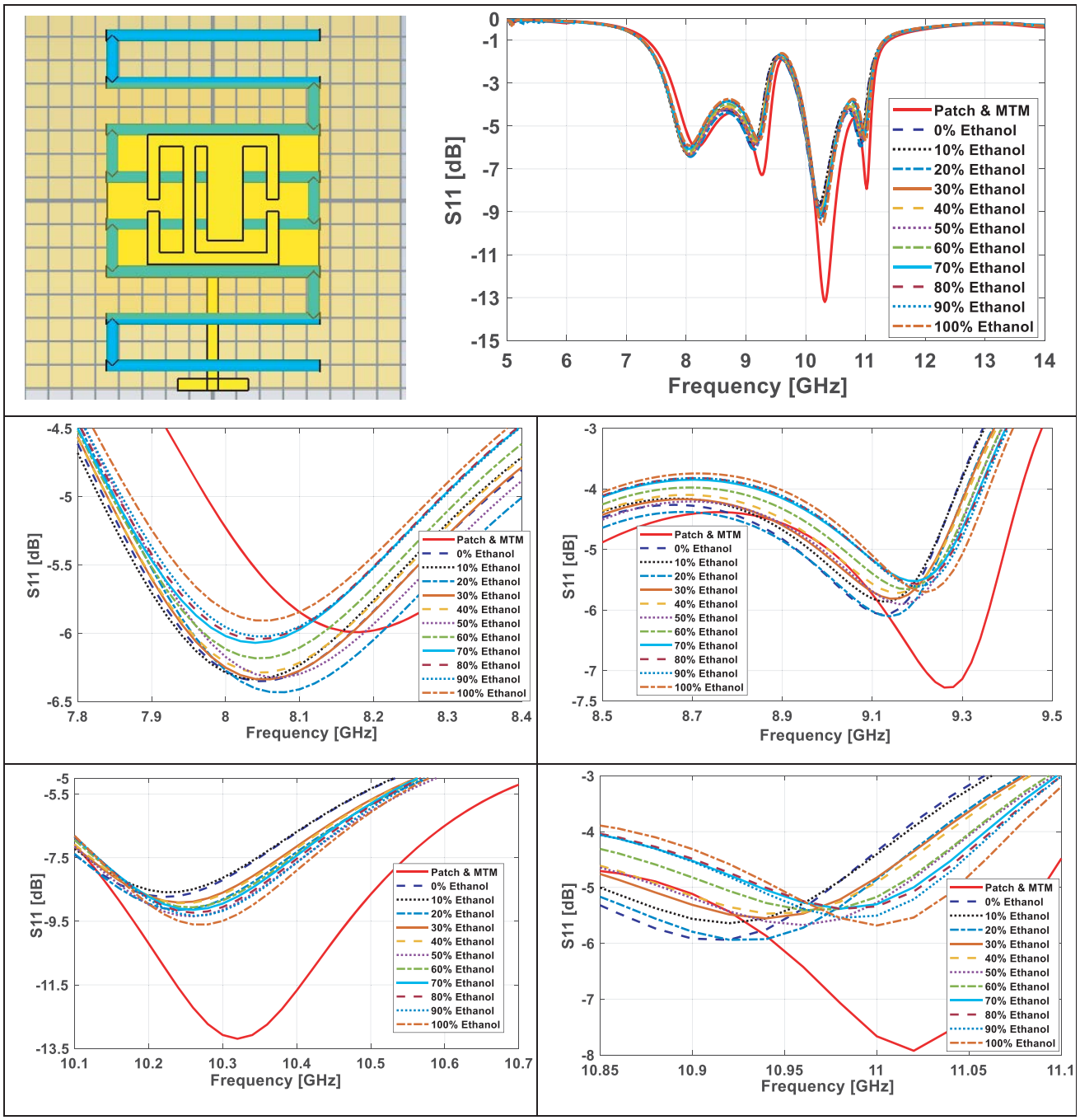

Figure 13. An optimized MTM 8-line fluidic channel sensor system and their sensing responses on different ethanol concentrations.

4. MULTI-NRI BAND MTM MICROFLUIDIC CHANNEL SENSORS

The NRI MTM was placed on top of the 1-line, 3-line and 4-line fluidic channels, shown in Figure 8. The sensor set consisted of three main layers of a patch antenna, microfluidic channel, and a MTM-enhancer, respectively. The fluidic channel location was adjusted to optimize the sensing responses.

Adding the MTM created two extra resonances in all three cases. Four resonances were observed in between 7.7–8.4 GHz, 8.5–9.5 GHz, 10.1–10.7 GHz, and 10.8–11.1 GHz, presented in Figures 9–11.

The disparity among the reflection coefficients from different ethanol samples was significantly noticeable as the number of channel lines increased to 3 and 4, respectively, which was noted at all four resonances.

In order to maximize the electric field perturbation, the microfluidic channel must be loaded where the strongest electric field is generated [12]. The fluidic channel was then further optimized in order to cover all sensing areas to create the best sensing responses, as well as to ensure a constant volume and shape of the fluid sample. Figures 12–13 present the other two optimized cases and their reflection coefficients.

The fluidic channel of the optimized sensor case 1 (Figure 12) was designed to fit inside the patch area. Although the testing fluid volume was reduced by almost half, this sensor set still demonstrated a great sensitivity. The best results were found in the second optimized sensor (Figure 13). 2-line channel meanders were added to both ends of the first optimized channel case. All four resonances clearly stressed the distinction of the ethanol of different concentrations.

5. CONCLUSION

Alternative metamaterial-inspired microwave microfluid sensors are designed to classify dielectric fluids with different concentrations. The multi-negative index bands generated by an I-beam metamaterial structure electrically and magnetically couple with the testing fluids, resulting in four distinct resonances. The differences from the reflection responses of the resonances are sufficient to distinguish the fluid types.

REFERENCES

1. Zhou, H., D. Hu, C. Yang, C. Chen, J. Ji, M. Chen, Y. Chen, Y. Yang, and Z. Mu, "Multi-band sensing for dielectric property of chemical using metamaterial integrated microfluidic sensor," *Scientific Reports*, Vol. 8, 14801, 2018.
2. Salim, A. and S. Lim, "Review of recent metamaterials microfluidic sensors," *Sensor*, Vol. 18, 232, 2018.
3. Weina, L., S. Haoran, and L. Xu, "A microwave method for dielectric characterization measurement of small liquids using a metamaterial-based sensor," *Sensor*, Vol. 18, 1438, 2018.
4. Bakır, M., M. Karaaslan, E. Unal, F. Karadag, F. O. Alkurt, O. Altıntaş, S. Dalgac, and C. Sabah, "Microfluidic and fuel adulteration sensing by using chiral metamaterial sensor," *J. Electrochem. Soc.*, Vol. 165, 11, 2018.
5. Su, L., J. Mata-Contreras, P. Velez, and F. Martin, "A review of sensing strategies for microwave sensors based on metamaterial-inspired resonator: Dielectric characterization, displacement, and angular velocity measurements for health diagnosis, telecommunication, and space applications," *Int. J. of Antennas and Propagation*, 5619728, 2017.
6. Velez, P., L. Su, K. Grenier, J. Mata-Contreras, D. Dubuc, and F. Martin, "Microwave microfluidic sensor based on a microstrip splitter/combiner configuration and split ring resonator for dielectric characterization of liquids," *IEEE Sensors Journal*, Vol. 17, 20, 2017.
7. Bakir, M., "Electromagnetic-based microfluidic sensor applications," *J. Electrochem. Soc.*, Vol. 164, B488–B494, 2017.
8. Shih, K., P. Pitchappa, M. Manjappa, C. P. Ho, R. Singh, and C. Lee, "Microfluidic metamaterial sensor: Selective trapping and remote sensing of microparticles," *J. Appl. Phys.*, Vol. 121, 023102, 2017.

9. Saghati, A. P., J. S. Batra, J. Kameoka, and K. Entesari, "A metamaterial-inspired wideband microwave interferometry sensor for dielectric spectroscopy of liquid chemicals," *IEEE Trans. Microw. Theory Tech.*, Vol. 65, 2558–2570, 2017.
10. Sadeqi, A. and S. Sonkusale, "Low-cost metamaterial-on-paper chemical sensor," *Transducers Int. Conf. Solid-State Sens., Actuators Microsyst.*, Vol. 25, 1437–1440, 2017.
11. Awang, R. A., F. J. Tovar-Lopez, T. Baum, S. Sriram, and W. S. T. Rowe, "Meta-atom microfluidic sensor for measurement of dielectric properties of liquids," *J. Appl. Phys.*, Vol. 121, 094506, 2017.
12. Salim, A. and S. Lim, "Complementary split-ring resonator-loaded microfluidic ethanol chemical sensor," *Sensors*, Vol. 16, 1802, 2016.
13. Kim, H. K., D. Lee, and S. A. Lim, "Fluidically tunable metasurface absorber for fexible large-scale wireless ethanol sensor applications," *Sensors*, Vol. 16, 1246, 2016.
14. Long, J. and B. Wang, "A metamaterial-inspired sensor for combined inductive-capacitive," *Appl. Phys. Lett.*, Vol. 106, 074104, 2015.
15. Kim, H. K., M. Yoo, and S. Lim, "Novel ethanol chemical sensor using microfluidic metamaterial," *Proceedings of the IEEE International Symposium on Antennas and Propagation & National Radio Science Meeting*, 1358–1359, Vancouver, BC, Canada, Jul. 2015.
16. Byford, J. A., K. Y. Park, and P. Chahal, "Metamaterial inspired periodic structure used for microfluidic sensing," *Proceedings of the Electronic Components Technology Conference*, 1997–2002, San Diego, CA, USA, May 2015.
17. Rawat, V., S. Dhobale, and S. N. Kale, "Ultra-fast selective sensing of ethanol and petrol using microwave-range metamaterial complementary split-ring resonators," *J. Appl. Phys.*, Vol. 116, 164106, 2014.
18. Ebrahimi, A., W. Withayachumnankul, S. Al-Sarawi, and D. Abbott, "High-sensitivity metamaterial-inspired sensor for microfluidic dielectric characterization," *IEEE Sensors Journal*, Vol. 14, No. 5, 2014.
19. Abduljabar, A., D. J. Rowe, A. Porch, and D. A. Barrow, "Novel microwave microfluidic sensor using a microstrip split-ring resonator," *IEEE Trans. Microw. Theory Tech.*, Vol. 62, 679–688, 2014.
20. Withayachumnankul, W., K. Jaruwongrungsee, A. Tuantranont, C. Fumeaux, and D. Abbott, "Metamaterial-based microfluidic sensor for dielectric characterization," *Sensors and Actuators A: Physical*, Vol. 189, 233–237, 2013.
21. Chretiennot, T., D. Dubuc, and K. Grenier, "A microwave and microfluidic planar resonator for efficient and accurate complex permittivity characterization of aqueous solutions," *IEEE Trans. Microw. Theory Techn.*, Vol. 61, No. 2, 972–978, 2013.
22. Agarwal, S. and Y. K. Prajapati, "Multifunctional metamaterial surface for absorbing and sensing applications," *Optics Communications*, Vol. 439, No. 15, 304–307, 2019.
23. Agarwal, S., Y. K. Prajapati, and V. Mishra, "Thinned fibre bragg grating as a fuel adulteration sensor: Simulation and experimental study," *Opto-Electronics Review*, Vol. 23, No. 4, 231–238, 2015.
24. Afapour, Z. O. V., Y. A. H. Ajati, and M. O. H. Ajati, "Graphene-based mid-infrared biosensor," *J. Opt. Soc. Am. B*, Vol. 34, 2586–2592, 2017.
25. Geng, Z., X. Zhang, Z. Fan, X. Lv, and H. Chen, "A route to terahertz metamaterial biosensor integrated with microfluidics for liver cancer biomarker testing in early stage," *Sci. Rep.*, Vol. 7, 1–11, 2017.
26. Sreekanth, K. V., Y. Alapan, M. El Kabbash, E. Ilker, M. Hinczewski, U. A. Gurkan, A. De Luca, and G. Strangi, "Extreme sensitivity biosensing platform based on hyperbolic metamaterials," *Nat. Mater.*, Vol. 15, 621–627, 2016.
27. Aristov, A. I., M. Manousidaki, A. Danilov, K. Terzaki, C. Fotakis, M. Farsari, and A. V. Kabashin, "3D plasmonic crystal metamaterials for ultra-sensitive biosensing," *Sci. Rep.*, Vol. 6, 1–8, 2016.
28. Chen, M., F. Fan, S. Shen, X. Wang, and S. Chang, "Terahertz ultrathin film thickness sensor below $\lambda/90$ based on metamaterial," *Appl. Opt.*, Vol. 55, 6471–6474, 2016.

29. Lee, D.-K. K., J.-H. H. Kang, J.-S. S. Lee, H.-S. S. Kim, C. Kim, J. Hun Kim, T. Lee, J.-H. H. Son, Q.-H. H. Park, and M. Seo, "Highly sensitive and selective sugar detection by terahertz nano-antennas," *Sci. Rep.*, Vol. 5, 1–7, 2015.
30. Wu, P. C., G. Sun, W. T. Chen, K. Y. Yang, Y. W. Huang, Y. H. Chen, H. L. Huang, W. L. Hsu, H. P. Chiang, and D. P. Tsai, "Vertical split-ring resonator based nanoplasmonic sensor," *Appl. Phys. Lett.*, Vol. 105, 3898, 2014.
31. Torun, H., F. Cagri Top, G. Dundar, and A. D. Yalcinkaya, "An antenna-coupled split-ring resonator for biosensing," *J. Appl. Phys.*, Vol. 116, 124701, 2014.
32. Lee, H. J., J. H. Lee, H. S. Moon, I. S. Jang, J. S. Choi, J. G. Yook, and H. Jung, "A planar split-ring resonator-based microwave biosensor for label-free detection of biomolecules," *Sens. Actuators B Chem.*, Vol. 169, 26–31, 2012.
33. Chen, T., S. Li, and H. Sun, "Metamaterials application in sensing," *Sensors*, Vol. 12, 2742–2765, 2012.
34. Zijlstra, P., P. M. R. Paulo, and M. Orrit, "Optical detection of single non-absorbing molecules using the surface plasmon resonance of a gold nanorod," *Nat. Nanotechnol.*, Vol. 7, 379–382, 2012.
35. Lee, H. J. and J. G. Yook, "Biosensing using split-ring resonators at microwave regime," *Appl. Phys. Lett.*, Vol. 92, 10–13, 2008.
36. White, G. M., "The origins and the future of microfluidics," *Nature*, Vol. 442, 368–373, 2006.
37. Su, L., J. Naqui, J. Mata-Contreras, and F. Martín, "Modeling metamaterial transmission lines loaded with pairs of coupled split ring resonators," *IEEE Antennas Wireless Propag. Lett.*, Vol. 14, 68–71, 2015.
38. Su, L., J. Naqui, J. Mata-Contreras, and F. Martín, "Modeling and applications of metamaterial transmission lines loaded with pairs of coupled complementary split ring resonators (CSRRs)," *IEEE Antennas Wireless Propag. Lett.*, Vol. 15, 154–157, 2016.
39. Su, L., J. Naqui, J. Mata-Contreras, and F. Martín, "Splitter/combiner microstrip sections loaded with pairs of complementary split ring resonators (CSRRs): Modeling and optimization for differential sensing applications," *IEEE Trans. Microw. Theory Techn.*, Vol. 64, No. 12, 4362–4370, Dec. 2016.
40. Su, L.., J. Mata-Contreras, and F. Martín, "Configurations of splitter/combiner microstrip sections loaded with stepped impedance resonators (SIRs) for sensing applications," *Sensors*, Vol. 16, No. 12, 2195, 2016.
41. Pendry, J. B., A. J. Holden, D. J. Robbins, and W. J. Stewart, "Magnetism from conductors and enhanced nonlinear phenomena," *IEEE Trans. Microw. Theory Techn.*, Vol. 47, No. 11, 2075–2084, 1999.
42. Sonsilphong, A. and N. Wongkasem, "Three-dimensional artificial double helices with high negative refractive index," *Journal of Optics*, Vol. 14, 105103, 2012.
43. Panpradit, W., A. Sonsilphong, C. Soemphol, and N. Wongkasem, "High negative refractive index chiral metamaterials," *Journal of Optics*, Vol. 14, 075101, 2012.
44. Matra, K. and N. Wongkasem, "Left-handed chiral isotropic metamaterials: Analysis and detailed numerical study," *Journal of Optics A: Pure and Applied Optics, Artificial Chiral Materials*, Vol. 11, 074011, 2009.
45. Sonsilphong, A. and N. Wongkasem, "Mid-infrared circular polarization switching in helical metamaterials," *Journal of Optics*, Vol. 18, 115102, 2016.
46. Sonsilphong, A., P. Gutruf, W. Withayachumnankul, D. Abbott, M. Bhaskaran, S. Sriram, and N. Wongkasem, "Flexible bi-layer terahertz chiral metamaterials," *Journal of Optics*, Vol. 17, 085101, 2015.
47. Fang, L., M. Wei, N. Wongkasem, H. Jaradat, A. Mokhlis, J. Shen, A. Akyurtlu, K. Marx, C. Barry, and J. Mead, "Tin assisted transfer of electroplated metal nanostructures and its application in flexible chiral metamaterials," *Microelectronic Engineering*, Vol. 107, 42–49, 2013.
48. Soemphol, C., S. F. Kitchin, M. A. Fiddy, and N. Wongkasem, "Electromagnetic responses of curved fishnet structures: Near-zero refractive index with lower loss," *Journal of Optics*, Vol. 18,

025102, 2016.

49. Soemphol, C., A. Sonsilphong, and N. Wongkasem, "Metamaterials with near-zero refractive index produced using fishnet structures," *Journal of Optics*, Vol. 16, 015104, 2013.
50. Mohammadia, A., A. Ismaila, M. A. Mahdia, R. S. A. R. Abdullaha, M. M. Isab, and A. R. Sadrolhosseinic, "Carbon-nanotube-based FR-4 patch antenna as a bio-material sensor," *Procedia Engineering*, Vol. 41, 724–728, 2012.
51. Bao, J. Z., M. L. Swicord, and C. C. Davis, "Microwave dielectric characterization of binary mixtures of water, methanol, and ethanol," *J. Chem. Phys.*, Vol. 104, 4441, 1996.
52. Pendry, J. B., A. J. Holden, W. J. Stewart, and I. Youngs, "Extremely low frequency plasmons in metallic mesostructures," *Phys. Rev. Lett.*, Vol. 76, 4773, 1996.
53. Smith, D. R., W. J. Padilla, D. C. Vier, S. C. Nemat-Nasser, and S. Schultz, "A composite medium with simultaneously negative permeability and permittivity," *Phys. Rev. Lett.*, Vol. 84, 4184–4187, 2000.
54. Katsarakis, N., T. Koschny, M. Kafesaki, E. N. Economou, and C. M. Soukoulis, "Electric coupling to the magnetic resonance of split ring resonators," *Appl. Phys. Lett.*, Vol. 84, No. 15, 2943–2945, 2004.
55. Rosa, E. B., *Bulletin of the Bureau of Standards*, Vol. 4, 301–344, Washington Government Printing Office, Washington D.C., 1908.
56. Vendik, O. G., S. P. Zubko, and M. A. Nikol'skii, "Modeling and calculation of the capacitance of a planar capacitor containing a ferroelectric thin film," *Tech. Phys.*, Vol. 44, No. 4, 349–355, 1999.
57. Arritt, B. J., D. R. Smith, and T. Khraishi, "Equivalent circuit analysis of metamaterial strain-dependent effective medium parameters," *J. of Applied Science*, Vol. 109, 073512, 2011.
58. Mackay, T. G., "Plane waves with negative phase velocity in isotropic chiral mediums," *Microw. Opt. Tech. Lett.*, Vol. 45, No. 2, 120–1, 2005.
59. Mackay, T. G. and A. Lakhtakia, "Simultaneous negative and positive phase-velocity propagation in an isotropic chiral medium," *Microw. Opt. Tech. Lett.*, Vol. 49, No. 6, 1245–6, 2007.
60. Wongkasem, N. and A. Akyurtlu, "Light splitting effects in chiral metamaterials," *Journal of Optics*, Vol. 12, 035101, 2010.